Article

An In Situ Reflectance Spectroscopic Investigation to Monitor Two-Dimensional MoS₂ Flakes on a Sapphire Substrate

Yina Wang[iD]**, Lei Zhang** *[iD]**, Wen Yang, Shanshan Lv, Chenhui Su, Hang Xiao, Faye Zhang, Qingmei Sui, Lei Jia and Mingshun Jiang**

School of Control Science and Engineering, Shandong University, Jingshi Road, Jinan 250061, China; ynwangsdu@163.com (Y.W.); wenyang0@126.com (W.Y.); sdulvshanshan@163.com (S.L.); suchenhui2010@163.com (C.S.); 15275139781@163.com (H.X.); zhangfaye@sdu.edu.cn (F.Z.); sdusqm@126.com (Q.S.); sdujial@126.com (L.J.); sdujiangmingshun@163.com (M.J.)

* Correspondence: drleizhang@sdu.edu.cn

check for updates

Abstract: In this work, we demonstrate the application of differential reflectance spectroscopy (DRS) to monitor the growth of molybdenum disulfide (MoS₂) using chemical vapor deposition (CVD). The growth process, optical properties, and structure evolution of MoS₂ were recorded by in-situ DRS. Indeed, blue shifts of the characteristic peak B were discussed with the decrease of temperature. We also obtained the imaginary part of the MoS₂ dielectric constant according to reflectance spectra. This method provides an approach for studying the change of two-dimensional (2D) materials' dielectric constant with temperature. More importantly, our work emphasizes that the DRS technique is a non-destructive and effective method for in-situ monitoring the growth of 2D materials, which is helpful in guiding the preparation of 2D materials.

Keywords: differential reflectance spectroscopy (DRS); in situ; molybdenum disulfide (MoS₂); sapphire substrate; chemical vapor deposition (CVD)

1. Introduction

Transition metal dichalcogenides (TMDCs) have attracted unprecedented attention in the last few years. As layered thin-film materials, two-dimensional (2D) TMDCs have massive advantages of the adjustable band gap, high carrier mobility, and excellent mechanical properties [1–4]. Molybdenum disulfide (MoS₂) is one of the most popular 2D TMDCs materials. The monolayer MoS₂ has a direct band-gap, which is between graphene with zero band-gap and hexagonal boron nitride with wide band-gap. It is considered to have attractive prospects for sensors, catalysis, supercapacitor, and optoelectronic devices [5–11]. It is crucial to acquire high-quality materials for industrial applications. Nevertheless, the research on the controllable preparation of high-quality materials still needs to be investigated. It is of great significance to explore the growth process and mechanisms of 2D materials for realizing the controllable preparation of thin 2D materials. Moreover, the interactions between substrates and materials can affect the structure and the growth status of the materials [12–14]. For instance, surface properties of substrates have an impact on the charge doping and strain for materials [14]. The transparent substrates, such as sapphire, mica, and quartz, are generally used as growth substrates of 2D materials. However, a systematic investigation of the growth mechanism on transparent substrates is still in the embryonic stage.

The in-situ observations during the growth of 2D materials have considerable advantages in analyzing the growth mechanisms. Ringe and collaborators observed in situ changes of TMDCs

optical properties during electroablation using spectroelectrochemical micro-extinction spectroscopy (SE-MExS) [15]. CVD is considered to be the most potential preparation technology to obtain high-quality materials among many preparation methods for 2D materials [14,16]. Nonetheless, there are limited reported on in-situ characterizations of CVD in the published literatures [17–20]. Wang et al. introduced the in-situ observation of monolayer molybdenum disulfide synthesized on a SiO_2/Si substrate by Raman spectroscopy and in situ images [17]. Kasırga's group explored the process of the salt-assisted TMDCs growth through optical micrographs using the modified CVD chamber [18]. Nevertheless, most of these reports emphasized the growth variation of 2D materials on opaque substrates because of the outstanding optical contrast, especially SiO_2/Si substrate. Sun's team used transmission spectroscopy to report the growth of molybdenum disulfide on the sapphire substrate [19]. They studied the significance of transmission spectra characterization for online growth detection and ignored the influence of the scattering on the spectra. More importantly, this research elucidates that the optical characterization technique is a powerful tool for detecting CVD-grown 2D materials. Differential reflectance spectroscopy (DRS) is a kind of optical detection technology with high sensitivity [20–22]. The DRS detection system is easy to set up and can be used to characterize variations on the substrate surface. Therefore, we can utilize DRS to investigate the evolution of as-grown 2D materials on the transparent substrate.

Here, as-grown CVD MoS_2 flakes on the transparent sapphire substrate were explored. The evolution of MoS_2 optical performances during the growth period was monitored by the in situ DRS. It was found that the position of the characteristic peak B shifted blue with a decrease of temperature. Meanwhile, the structure of MoS_2 flakes was also characterized by the imaginary part of the dielectric constant. Our results showed a variation of the imaginary part of the dielectric constant with temperature for MoS_2 flakes. Additionally, optical microscopy, Raman spectra, ex-situ DRS, and atomic force microscopy (AFM) were ex-situ conducted to verify the formation of MoS2 flakes at room temperature.

2. Materials and Methods

2.1. CVD Growth of MoS₂ Flakes on the Sapphire Substrate

The atmospheric pressure CVD (APCVD) was used to prepare the MoS_2 flakes on the single-crystalline sapphire (0001) substrate. The sample was synthesized in a tubular furnace with two temperature zones. High purity sulfur powder (1.0 g, 99.99 wt%, Alfa Aesar, Shanghai, China) and MoO_3 powder (15 mg, 99.99 wt%, Alfa Aesar, Shanghai, China) were supplied as two precursors for the growth of MoS_2. The MoO_3 power was placed on the alumina boat, which was located 6.0 cm upstream from a sapphire substrate in the second temperature zone of the tube furnace. Another alumina boat with sulfur power was put in the first temperature zone. First, the air in the reaction chamber was evacuated by a vacuum pump, and then the reaction chamber was filled with high-purity argon to the atmospheric pressure. After that, we continued to ventilate into the furnace for 5 min to remove air as much as possible. Subsequently, MoO_3 powder was heated to 600 °C in 30 min. Afterward, it continued to be ramped to 800 °C in 30 min and maintained for 40 min. Finally, the furnace was naturally cooled down to room temperature. During the growth condition, argon gas as the carrier gas was injected into a reaction chamber to convey vapor of precursors to the down-stream substrate.

2.2. In Situ Characterization

For the in-situ characterization experiment, original reflected intensity data was collected by the homemade online optical system. The detailed process can be found in Reference [20]. In situ DRS technology is utilized to process the reflected intensity, and it is expressed by:

$$\frac{\Delta R}{R} = \frac{R_f(T_i) - R_s(T_i)}{R_s(T_i)}, \tag{1}$$

where $R_s(T_i)$ and $R_f(T_i)$ denote the reflected intensity of the bare substrate and one of CVD grown flakes at the same temperature T_i. It is necessary to gather the reflected intensity $R_s(T_i)$ of the bare substrate with the whole temperature range before the TMDCs preparation. The schematic illustration of the in-situ DRS model displays in Figure 1. By the above-mentioned data processing, in-situ DRS values can effectively suppress the influence of high temperature on growth information. This makes DRS an optical probe technique for characterizing TMDCs prepared by CVD. Additionally, this method is suitable under conditions that the gas atmosphere has no absorption properties and the detected material has optical absorption in the measurement wavelength range.
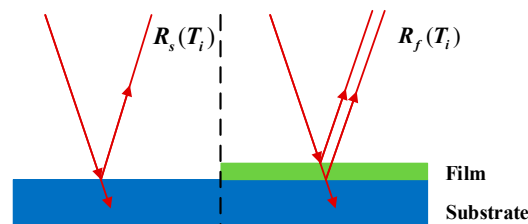

Figure 1. The schematic diagram of in-situ DRS model in the variable temperature environment.

2.3. Ex Situ Measurements

MoS$_2$ flakes prepared on the sapphire substrate were systematically off-line measured by optical microscope, Raman spectra, ex-situ DRS, and atomic force microscope (AFM). These measurements were operated at room temperature. Firstly, optical images were obtained with an optical microscope (GFM-550, Shanghai Guangmi Instrument Co., Ltd., Shanghai, China). Secondly, Raman spectra were used to evaluate the quality and structure of the sample by Raman microscope (HR Evolution 800, Horiba, Paris, France). A ×50 objective lens and the excitation wavelength of 532 nm were used. Afterward, ex-situ DRS at room temperature were obtained by $DRS = (R_F - R_0)/R_0$, where R_F and R_0 represent the reflected intensity of the substrate surfaces covered with and without MoS$_2$ flakes, respectively. At last, the thickness of MoS$_2$ flakes was acquired by an AFM (Dimension Icon, Bruker, Santa Barbara, CA, USA) in PeakForce tapping mode.

2.4. Calculation of Dielectric Constant

Based on the Fresnel formula, we can establish a relationship between the DRS values and the dielectric constant of the material [23]. When a substrate is transparent within the measured light range, the imaginary parts of the extinction coefficient and dielectric constant for the substrate are equal to zero. Therefore, the imaginary part ε'' of MoS$_2$ dielectric constant can be calculated from DR values, defined as: [21,24]

$$\varepsilon'' = \frac{DR \cdot \left(1 - n_s^2\right)\lambda}{8\pi d_f}, \tag{2}$$

where n_s is the refractive index of the substrate, λ is the wavelength of detection light, and d_f is the average thickness of flakes on the substrate. In addition, d_f is defined by $d_f = d \cdot \theta_f$, where d denotes the thickness of monolayer MoS$_2$ and θ_f represents the partial coverage of the observation area on the substrate. As a result, the ε'' data is the characteristic of the material on the substrate with a coverage of θ_f. Here, the thickness of the sample is acquired by AFM and the coverage is deduced by optical microscopy images.

3. Results and Discussion

3.1. In Situ Reflectance Spectroscopy

We prepared MoS$_2$ flakes on the sapphire substrate by CVD using MoO$_3$ and sulfur as precursors. The reverse side of a sapphire substrate was roughened to avoid interference influence [25]. In order to

get a deep insight into the formation of the MoS_2 flakes, we employed the DRS technique to monitor the overall evolution during the growing MoS_2 on the sapphire substrate. As illustrated in Figure 2a, the entire experimental process is divided into three sections by temperature variations: heating, holding, and cooling sections. With a close inspection in Figure 2b, the $\Delta R/R$ signals are plotted every 100 °C for the heating section. It is essential to point out that the optical absorption performance hardly appears in Figure 2b. One can deduce that there are almost no MoS_2 flakes covering the substrate surface for this section, which can be attributed that the temperature of the furnace was relatively low. Thus, the spectra of the heating section display no distinct characteristic peaks of MoS_2 flakes. Figure 2c shows the evolution of DRS signals during the holding section, in which the spectrum is drawn every 8 min. The absorption peak around 2.70 eV gradually becomes prominent with the increase of time. This peak is consistent with the MoS_2 characteristic peak called C peak, which is related to van Hove singularity. It can be interpreted by the broad spectral transition between K and Γ in the Brillouin region, where the conduction bands are almost parallel to the valence bands [26]. Compared with other absorption peaks, the peak C is more easily observed. It could be related that van Hove singularity can enhance the interaction between light and matter and result in photon absorption enhancement [27]. Notably, the red-shift of peak C occurred due to higher temperatures compared with room temperature. Furthermore, the sudden changes of DRS intensity near 77 min and 85 min are associated with the thermal deformation of mechanical structures, such as the sample stage. In-situ DRS during the cooling section are plotted per every 100 °C in Figure 2d. There are three characteristic peaks of MoS_2 corresponding to peak A, B, and C. As the experiment progressed, the two characteristic peaks A and B located at 1.86 eV and 2.01 eV gradually appeared respectively. They arise from the exciton transitions of K point in the Brillouin region. The energy difference between peak A and B can be attributed to the valence band separation caused by spin-orbit coupling [28]. In addition, as illustrated in the insertion graph of Figure 2d, the peak B had blue shifts with the decrease of temperature. It comes from the increased overlap of orbits that form the band during the cooling section [29]. This observation provides direct evidence that the absorption features of MoS_2 flakes are affected by temperature.

On the basis of the investigation above, a closer inspection of the incremental DRS signals is exhibited in Figure 3. As one can see from Figure 3a, the alteration of $\Delta(\Delta R/R)$ spectrum is slight for the heating section. It can be speculated that MoS_2 domains have hardly been formed. In Figure 3b, there is a prominent peak at 2.70 eV in the $\Delta(\Delta R/R)$ spectrum during the holding section. It can be inferred that the surface of the sapphire substrate has been covered with MoS_2 flakes. For the cooling section sketched in Figure 3c, the increment of DRS reveals distinct peaks corresponding to the characteristic peaks A, B, and C of MoS_2 flakes, respectively. Note that this result has also provided direct evidence for the growth of MoS_2 flakes. Furthermore, we also calculated the dielectric constant to analyze the growth process of MoS_2. Figure 3d shows the imaginary parts ε'' of the MoS_2 dielectric constant at different temperatures. The amplitudes are slightly different compared with the literature due to different measurement methods and the effect of sample uniformity [16]. More importantly, it can be recognized that the peaks of ε'' also are blue-shifted with the decrease of temperature, which can be attributed to the reduced electron-phonon interaction and the decrement of lattice constant [30,31]. Consequently, the detailed growth evolution of MoS_2 flakes can be revealed from in-situ reflection spectra and their increments.
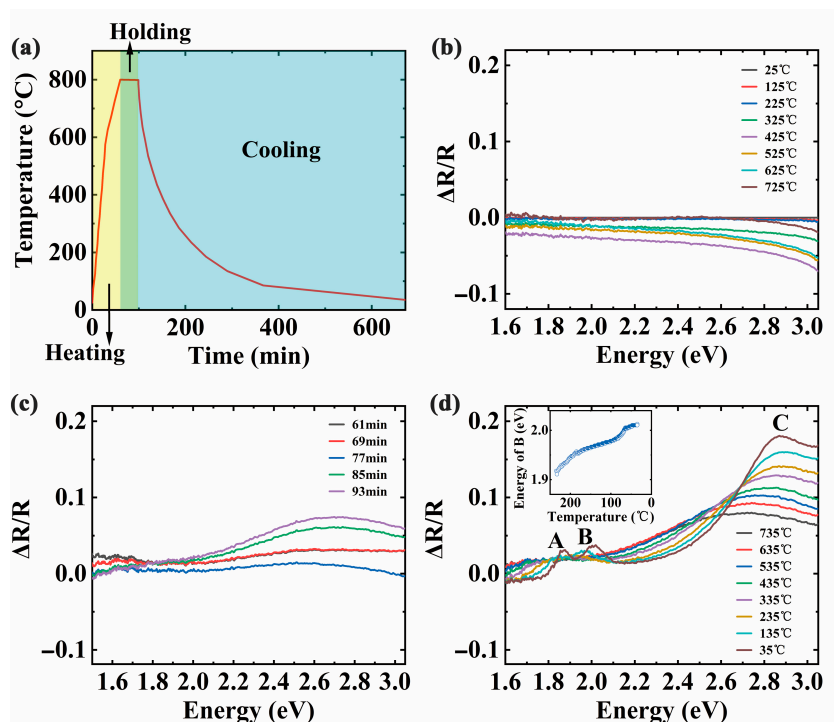
Figure 2. (**a**) The temperature profile during the growth of molybdenum disulfide (MoS$_2$) flakes using chemical vapor deposition (CVD); (**b**–**d**) In-situ differential reflectance spectroscopy (DRS) of the heating, holding, and cooling sections during the CVD growth, respectively. The inset in (**d**) is the variation of peak B with temperature. A, B, and C represent three characteristic peaks of MoS$_2$ at different energy, respectively.
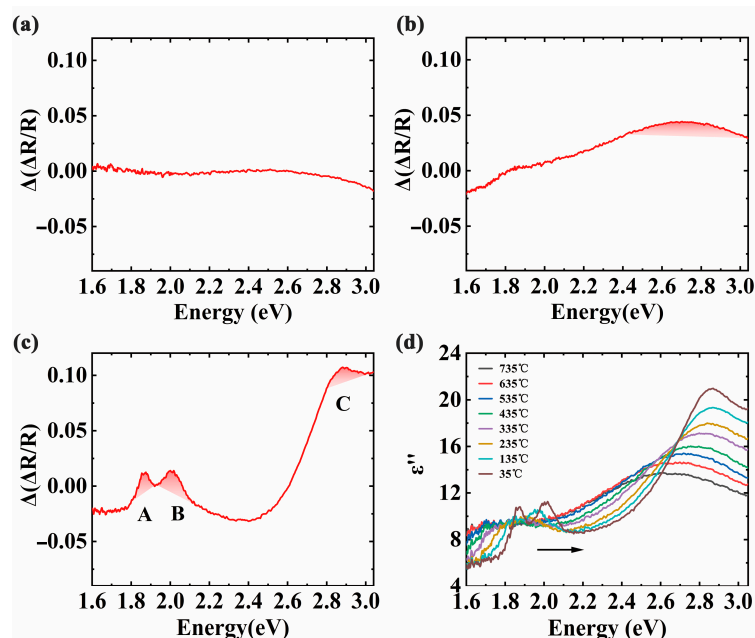

Figure 3. (**a**–**c**) The increments of DRS during heating, holding and cooling section for the CVD growth, respectively. A, B, and C represent three characteristic peaks of MoS$_2$ at different energy, respectively; (**d**) The imaginary part values ε'' of MoS$_2$ dielectric constant per 100 °C during the cooling section. The arrow indicates the direction of the peak as the temperature decreases.

3.2. Ex-Situ Characterization

To further probe the morphology and structure of the MoS$_2$ flakes, optical microscopy, Raman spectroscopy, ex-situ DRS, and AFM were performed at room temperature, respectively. Figure 4a displays the optical image of the sample on the sapphire substrate, which reveals the triangular morphology of MoS$_2$ flakes with flat surfaces. Their side lengths ranged from 10 to 30 μm in size. Raman characterization displays two characteristic peaks in Figure 4b. The peak E$^1_{2g}$ at 385.7 cm^{-1} is attributed to the in-plane vibration mode of MoS$_2$, while the peak A$_{1g}$ at 405.3 cm^{-1} is associated with the out-of-plane vibration mode. It is worth to mention that the frequency difference between the E$^1_{2g}$ and A$_{1g}$ is sensitive to the layer thickness. Raman frequency difference of MoS$_2$ flakes is ~19.6 cm^{-1}, in good agreement with that of monolayer MoS$_2$ in previous studies [32]. Thus, the thickness for the sample can be interpreted by a monolayer structure. Moreover, ex-situ DRS at room temperature is presented in Figure 4c. The absorption peaks A, B, and C of MoS$_2$ domains appear at 1.86 eV, 2.01 eV, and 2.83 eV, respectively. Additionally, AFM was used to assess the thickness of as-grown MoS$_2$ flakes on the sapphire. A height profile along the black broken line is about 0.85 nm in Figure 4d, which is consistent with the results of monolayer MoS$_2$ thickness reported in the literature [32,33]. An AFM image in the inset of Figure 4d reveals that the sample has the classic monolayer topography. Therefore, ex-situ characterization results confirm that MoS$_2$ flakes have synthesized on the sapphire substrate in accordance with that of in-situ DRS.
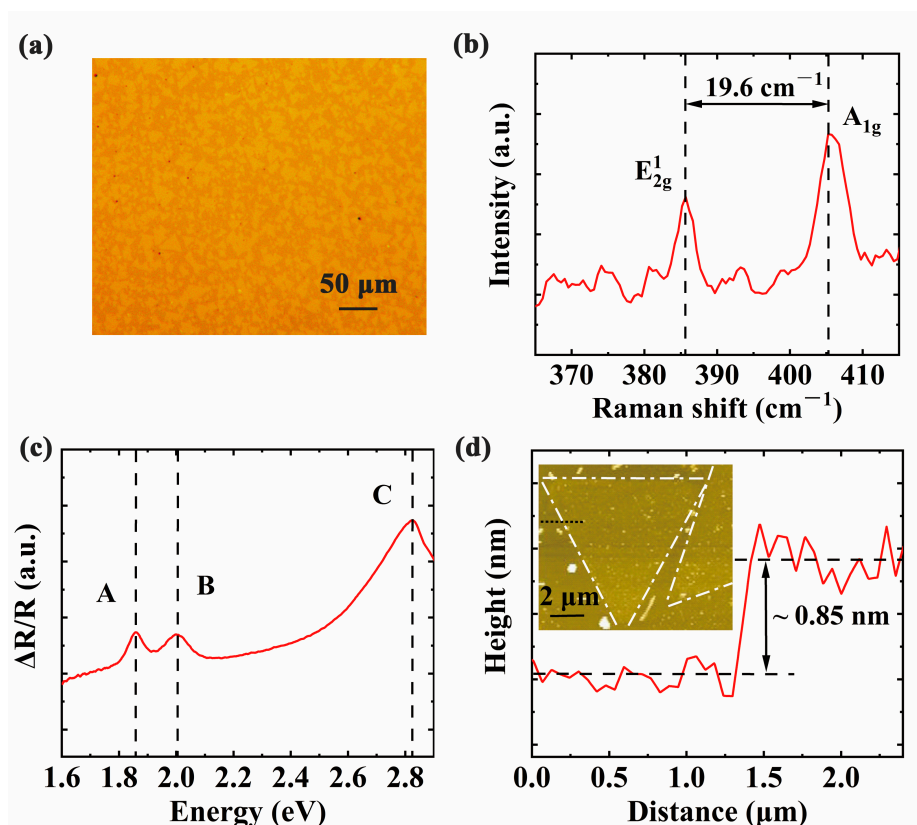

Figure 4. The ex-situ characterizations of the MoS$_2$ sample at room temperature. (**a**) An optical image of MoS$_2$ flakes on the sapphire substrate. The scale bar is 50 μm; (**b**,**c**) Raman spectra and DRS of MoS$_2$ flakes respectively. A, B, and C represent three characteristic peaks of MoS$_2$ at different energy, respectively.; (**d**) An atomic force microscopy (AFM) height profile recorded the triangular MoS$_2$ flakes along the black short-dot line. Triangular MoS2 flakes are marked with white dash-dot lines. The inset is the corresponding graph with the scale bar of 2 μm.

4. Conclusions

In summary, the growth process of MoS$_2$ flakes synthesized by CVD on the transparent sapphire substrate was in situ monitored. We adopted reflectance spectroscopy to successfully record the evolution of MoS$_2$ optical characteristics during CVD growth. Specifically, the growth of the MoS$_2$ flakes began in the holding section. It is worth mentioning that the characteristic peak C has more prominent absorption performance at higher temperatures compared to the absorption peak A and B. More importantly, blue shifts of peak B were recorded with the influence of temperature. In addition, the dielectric constant of MoS$_2$ was also obtained. This result can provide a method to observe the changes of dielectric constant for 2D materials with different temperatures. It is essential to point out that in situ DRS can also be applied to investigate the preparation of other 2D materials on the sapphire substrate. This work can contribute to a better understanding of the 2D materials growth mechanism and controllable synthesis.

References

1. Dumcenco, D.; Ovchinnikov, D.; Marinov, K.; Lazić, P.; Gibertini, M.; Marzari, N.; Sanchez, O.L.; Kung, Y.C.; Krasnozhon, D.; Chen, M.W.; et al. Large-area epitaxial monolayer MoS$_2$. *ACS Nano* **2015**, *9*, 4611–4620. [CrossRef]

2. Wang, Q.H.; Kalantar-Zadeh, K.; Kis, A.; Coleman, J.N.; Strano, M.S. Electronics and optoelectronics of two-dimensional transition metal dichalcogenides. *Nat. Nanotechnol.* **2012**, *7*, 699–712. [CrossRef]

3. Hien, N.D.; Nguyen, C.V.; Hieu, N.N.; Kubakaddi, S.S.; Duque, C.A.; Mora-Ramos, M.E.; Dinh, L.; Bich, T.N.; Phuc, H.V. Magneto-optical transport properties of monolayer transition metal dichalcogenides. *Phys. Rev. B* **2020**, *101*, 1–13. [CrossRef]

4. Butler, S.Z.; Hollen, S.M.; Cao, L.; Cui, Y.; Gupta, J.A.; Gutiérrez, H.R.; Heinz, T.F.; Hong, S.S.; Huang, J.; Ismach, A.F.; et al. Progress, challenges, and opportunities in two-dimensional materials beyond graphene. *ACS Nano* **2013**, *7*, 2898–2926. [CrossRef]

5. Ermolaev, G.A.; Stebunov, Y.V.; Vyshnevyy, A.A.; Tatarkin, D.E.; Yakubovsky, D.I.; Novikov, S.M.; Baranov, D.G.; Shegai, T.; Nikitin, A.Y.; Arsenin, A.V.; et al. Broadband optical properties of monolayer and bulk MoS$_2$. *npj 2D Mater. Appl.* **2020**, *4*, 1–6. [CrossRef]

6. Li, J.; Chen, Z.; Yang, H.; Yi, Z.; Chen, X.; Yao, W.; Duan, T.; Wu, P.; Li, G.; Yi, Y. Tunable broadband solar energy absorber based on monolayer transition metal dichalcogenides materials using au nanocubes. *Nanomaterials* **2020**, *10*, 257. [CrossRef]

7. Raza, A.; Ikram, M.; Aqeel, M.; Imran, M.; Ul-Hamid, A.; Riaz, K.N.; Ali, S. Enhanced industrial dye degradation using Co doped in chemically exfoliated MoS$_2$ nanosheets. *Appl. Nanosci.* **2020**, *10*, 1535–1544. [CrossRef]

8. Eda, G.; Maier, S.A. Two-dimensional crystals: Managing light for optoelectronics. *ACS Nano* **2013**, *7*, 5660–5665. [CrossRef]

9. Li, J.; Chen, X.; Yi, Z.; Yang, H.; Tang, Y.; Yi, Y.; Yao, W.; Wang, J.; Yi, Y. Broadband solar energy absorber based on monolayer molybdenum disulfide using tungsten elliptical arrays. *Mater. Today Energy* **2020**, *16*, 100390. [CrossRef]

10. Das, P.; Nash, J.; Webb, M.; Burns, R.; Mapara, V.N.; Ghimire, G.; Rosenmann, D.; Divan, R.; Karaiskaj, D.; McGill, S.A.; et al. High broadband photoconductivity of few-layered MoS$_2$ field-effect transistors measured using multi-terminal methods: Effects of contact resistance. *Nanoscale* **2020**, *12*, 22904–22916. [CrossRef]

11. Chai, C.; Tan, H.; Fan, X.; Huang, K. MoS$_2$ nanosheets/graphitized porous carbon nanofiber composite: A dual-functional host for high-performance lithium–sulfur batteries. *J. Alloys Compd.* **2020**, *820*, 153144. [CrossRef]

12. Yue, X.F.; Wang, Y.Y.; Zhao, Y.; Jiang, J.; Yu, K.; Liang, Y.; Zhong, B.; Ren, S.T.; Gao, R.X.; Zou, M.Q. Measurement of interfacial thermal conductance of few-layer MoS$_2$ supported on different substrates using Raman spectroscopy. *J. Appl. Phys.* **2020**, *127*, 104301. [CrossRef]

13. Buscema, M.; Steele, G.A.; van der Zant, H.S.J.; Castellanos-Gomez, A. The effect of the substrate on the Raman and photoluminescence emission of single-layer MoS$_2$. *Nano Res.* **2014**, *7*, 561–571. [CrossRef]

14. Chae, W.H.; Cain, J.D.; Hanson, E.D.; Murthy, A.A.; Dravid, V.P. Substrate-induced strain and charge doping in CVD-grown monolayer MoS$_2$. *Appl. Phys. Lett.* **2017**, *111*, 143106. [CrossRef]

15. Kumar, A.; Sebastian, A.; Das, S.; Ringe, E. In Situ Optical Tracking of Electroablation in Two-Dimensional Transition-Metal Dichalcogenides. *ACS Appl. Mater. Interfaces* **2018**, *10*, 40773–40780. [CrossRef]

16. Li, W.; Birdwell, A.G.; Amani, M.; Burke, R.A.; Ling, X.; Lee, Y.H.; Liang, X.; Peng, L.; Richter, C.A.; Kong, J.; et al. Broadband optical properties of large-area monolayer CVD molybdenum disulfide. *Phys. Rev. B Condens. Matter Mater. Phys.* **2014**, *90*, 1–8. [CrossRef]

17. Xue, H.; Wu, G.; Zhao, B.; Wang, D.; Wu, X.; Hu, Z. High-Temperature In Situ Investigation of Chemical Vapor Deposition to Reveal Growth Mechanisms of Monolayer Molybdenum Disulfide. *ACS Appl. Electron. Mater.* **2020**, *2*, 1925–1933. [CrossRef]

18. Rasouli, H.R.; Mehmood, N.; Çakıroğlu, O.; Kasırga, T.S. Real time optical observation and control of atomically thin transition metal dichalcogenide synthesis. *Nanoscale* **2019**, *11*, 7317–7323. [CrossRef] [PubMed]

19. López-posadas, C.B.; Wei, Y.; Shen, W.; Kahr, D.; Hohage, M.; Sun, L. Direct observation of the CVD growth of monolayer MoS$_2$ using in situ optical spectroscopy. *Beilstein J. Nanotechnol.* **2019**, *10*, 557–564. [CrossRef]

20. Wang, Y.; Zhang, L.; Su, C.; Xiao, H.; Lv, S.; Zhang, F.; Sui, Q.; Jia, L.; Jiang, M. Direct Observation of Monolayer MoS$_2$ Prepared by CVD Using In-Situ Differential Reflectance Spectroscopy. *Nanomaterials* **2019**, *9*, 1640. [CrossRef]

21. Forker, R.; Gruenewald, M.; Fritz, T. Optical differential reflectance spectroscopy on thin molecular films. *Annu. Rep. Sect. C Phys. Chem.* **2012**, *108*, 34. [CrossRef]

22. Zhang, L.; Hu, C.; Fu, X.; Jiang, M.; Sui, Q.; Jia, L. Pentacene crystal transition during the growth on SiO$_2$ studied by in situ optical spectroscopy. *Synth. Met.* **2017**, *231*, 65–69. [CrossRef]

23. McIntyre, J.D.E.; Aspnes, D.E. Differential reflection spectroscopy of very thin surface films. *Surf. Sci.* **1971**, *24*, 417–434. [CrossRef]

24. Forker, R.; Fritz, T. Optical differential reflectance spectroscopy of ultrathin epitaxial organic films. *Phys. Chem. Chem. Phys.* **2009**, *11*, 2142–2155. [CrossRef]

25. Wei, Y.; Hu, C.; Li, Y.; Hu, X.; Hohage, M.; Sun, L. Growth oscillation of MoSe$_2$ monolayers observed by differential reflectance spectroscopy. *J. Phys. Condens. Matter* **2020**, *32*, 155001. [CrossRef]

26. Baek, S.H.; Choi, Y.; Choi, W. Large-Area Growth of Uniform Single-Layer MoS$_2$ Thin Films by Chemical Vapor Deposition. *Nanoscale Res. Lett.* **2015**, *10*, 4–9. [CrossRef]

27. Britnell, L.; Ribeiro, R.M.; Eckmann, A.; Jalil, R.; Belle, B.D.; Mishchenko, A.; Kim, Y.J.; Gorbachev, R.; Georgiou, T.; Morozov, S.V.; et al. Strong Light-Matter Interactions Thin Films. *Science* **2013**, *340*, 1311–1315. [CrossRef]

28. Mak, K.F.; He, K.; Lee, C.; Lee, G.H.; Hone, J.; Heinz, T.F.; Shan, J. Tightly bound trions in monolayer MoS$_2$. *Nat. Mater.* **2013**, *12*, 207–211.

29. Yalon, E.; Aslan, Ö.B.; Smithe, K.K.H.; McClellan, C.J.; Suryavanshi, S.V.; Xiong, F.; Sood, A.; Neumann, C.M.; Xu, X.; Goodson, K.E.; et al. Temperature-Dependent Thermal Boundary Conductance of Monolayer MoS$_2$ by Raman Thermometry. *ACS Appl. Mater. Interfaces* **2017**, *9*, 43013–43020. [CrossRef]

30. Le, V.L.; Kim, T.J.; Park, H.G.; Nguyen, H.T.; Kim, Y.D.; Nguyen, H.T. Temperature dependence of the dielectric function of monolayer MoS$_2$. *Curr. Appl. Phys.* **2019**, *19*, 182–187. [CrossRef]

31. Park, H.G.; Kim, T.J.; Kim, H.S.; Yoo, C.H.; Barange, N.S.; Le, V.L.; Kim, H.U.; Senthilkumar, V.; Le, C.T.; Kim, Y.S.; et al. Temperature dependence of the critical points of monolayer MoS$_2$ by ellipsometry. *Appl. Spectrosc. Rev.* **2016**, *51*, 621–635. [CrossRef]

32. Han, T.; Liu, H.; Wang, S.; Chen, S.; Li, W.; Yang, X. Probing the Optical Properties of MoS$_2$ on SiO2/Si and Sapphire Substrates. *Nanomaterials* **2019**, *9*, 740. [CrossRef] [PubMed]

33.   Liu, H.; Si, M.; Najmaei, S.; Neal, A.T.; Du, Y.; Ajayan, P.M.; Lou, J.; Ye, P.D. Statistical study of deep submicron dual-gated field-effect transistors on monolayer chemical vapor deposition molybdenum disulfide films. *Nano Lett.* **2013**, *13*, 2640–2646. [CrossRef]

Publisher's Note: MDPI stays neutral with regard to jurisdictional claims in published maps and institutional affiliations.